European Journal of Neuroscience

Title: Temporal dynamics of oscillatory brain activity during the observation of communicative interactions between point-light agents

Elisabeth V. C. Friedrich*[1], Imme C. Zillekens[2,3], Anna Lena Biel[1], Dariusz O'Leary[1], Johannes Singer[1,4], Eva Victoria Seegenschmiedt[1], Paul Sauseng[1] & Leonhard Schilbach[2,3,5]

[1]Department of Psychology, Research Unit Biological Psychology, Ludwig-Maximilians-Universität München, Leopoldstr. 13, 80802 Munich, Germany
[2]Independent Max Planck Research Group for Social Neuroscience, Max Planck Institute of Psychiatry, Kraepelinstr. 2-10, 80804 Munich, Germany
[3]International Max Planck Research School for Translational Psychiatry, Kraepelinstr. 2-10, 80804 Munich, Germany
[4]Department of Education and Psychology, Freie Universitat Berlin, Berlin, 14195 Germany
[5]Medical Faculty, Ludwig-Maximilians-Universität München, Munich, 80802 Germany

*** Corresponding author:**
Elisabeth V. C. Friedrich
Research Unit Biological Psychology, Department of Psychology, LMU Munich
Leopoldstr. 13, 80802 Munich, Germany
Email: elisabeth.friedrich@psy.lmu.de
Phone: +49 (0) 89 / 2180 6159
Fax: +49 (0) 89 / 2180-3125

Abstract

Predicting actions from nonverbal cues and using them to optimize one's response behavior (i.e., interpersonal predictive coding) is essential in everyday life social interaction. 39 participants watched two agents depicted by moving point-light stimuli while an electroencephalogram (EEG) was recorded. One well-recognizable agent performed either a 'communicative' or an 'individual' action. The second agent was either masked by a cloud of noise dots, or absent and replaced by noise dots, which participants had to differentiate. EEG amplitude and coherence analyses for theta, alpha and beta frequency bands revealed a dynamic pattern unfolding over time: Watching communicative actions was associated with enhanced coupling within medial anterior regions involved in social and mentalizing processes and with dorsolateral prefrontal activation indicating a higher deployment of cognitive resources. Trying to detect the masked agent without having seen communicative cues was related to enhanced coupling in posterior regions for social perception and visual processing. Observing an expected outcome was associated with increased motor system activation. Finally, when the masked agent was detected correctly, activation in posterior areas for visual processing and social cognition was increased. Taken together, our results demonstrate that it is crucial to consider the temporal dynamics of social interactions and of their neural correlates to better understand interpersonal predictive coding.

Keywords

Electroencephalography (EEG); oscillations; amplitude and coherence analyses; interpersonal predictive coding; social cognition

INTRODUCTION

Predicting other people's actions from nonverbal cues and optimizing the response behavior accordingly is critical in social interactions. We interpret nonverbal cues from one person to infer upon the presence and consequent action of another person to whom the behavior is directed. This phenomenon has been described as *interpersonal predictive coding* (Manera, Becchio, *et al.*, 2011; Manera, del Giudice, *et al.*, 2011; von der Lühe *et al.*, 2016). It can be investigated with point-light displays of agents (i.e., humans represented only by moving dots, which are attached to their major joints) communicating with each other (Neri *et al.*, 2006; Pavlova, 2012). According to the idea of interpersonal predictive coding, the brain generates hypotheses about subsequent actions of a potential interaction partner when seeing one person's communicative gesture. When we see someone wave hello, we expect to see a second person, to whom this action is addressed. These interpersonal predictions are then compared to sensory input to make out whether, indeed, a second person is present or not. This can be especially important in noisy environments, e.g. to facilitate the detection of a masked point-light agent in a cloud of dots (Manera, Becchio, *et al.*, 2011).

In a functional magnetic resonance imaging (fMRI) study, Zillekens and colleagues (2019) used point-light agents to investigate the neural correlates of this phenomenon. They showed neuro-typical study participants a well recognizable point-light agent (agent A) and a second point-light agent masked by randomly moving noise dots (agent B) or no second agent at all, but only noise dots. First, participants watched agent A performing either an individual or a communicative gesture. Second, they focused on agent B's response action masked with a cloud of moving dots, or on noise dots that replaced agent B in 50% of the trials. Then, the participants had to indicate with a button press whether agent B had been present or absent in the cloud of moving dots. Behavioral results were in line with previous studies showing that communicative gestures, in contrast to individual actions, facilitated the perception of a second agent (Manera, del Giudice, *et al.*, 2011) and increased its detection probability (Manera, Becchio, *et al.*, 2011). On the neural level, the amygdala was found to be functionally coupled to the medial prefrontal cortex for communicative actions, a key region of the so-called mentalizing system of the brain, whose role for social cognition has repeatedly been demonstrated (Redcay and Schilbach, 2019). In the context of individual actions, the amygdala conversely showed increased connectivity to fronto-parietal areas, previously implicated as part of the attention system of the brain (Zillekens *et al.*, 2019).

Given its high spatial resolution, fMRI allows to localize specific cortical and subcortical brain regions contributing to an effect. However, a temporal differentiation of sub processes from observing nonverbal cues to the motor reaction to a specific gesture is not possible. Being able to analyze social interactions in distinct time segments is crucial,

however, as different cognitive processes might be involved at different time points. Moreover, splitting the task into time intervals enables us to investigate the initial processing of social gestures without confounding consequent factors such as matching or mismatching of predictions, the presence or absence of a second agent or trial outcome (Wurm and Caramazza, 2019). It also allows us to tie the time segments to specific events in the trial such as the response and, thus, our analyses of brain activity are not confounded by behavioral differences in reaction time for example.

In order to exploit these advantages, we therefore used EEG in combination with the established task to analyze the temporal dynamics of the cortical brain locations indicated by Zillekens and colleagues (2019) during interpersonal predictive coding (i.e., *a priori* based regions of interests (ROIs)). Additionally, we ran a data-driven whole brain analysis in order to see if further brain areas show specific activation for certain cognitive processes at a given time point. We hypothesized that different cognitive processes would be involved at different time points in this complex task of social interaction as used by Zillekens and colleagues (2019). To investigate our claim, we split the task into three different time segments indicative of different cognitive processes involved in the task:

In the time segment (1) before the onset of agent B's response action, participants focused on the well-recognizable agent A and viewed either a communicative or an individual gesture. In contrast to an individual gesture, a communicative action allowed the participants to form an immediate expectation for how agent B (if it was present) would act in response. Other studies have shown that the expectation of an upcoming action from someone else in a predictable context leads to an activation of one's own sensorimotor system cortex, which has been interpreted as potentially reflecting mirror neuron activity (Kilner *et al.*, 2004; Maranesi *et al.*, 2014; Krol *et al.*, 2020). The mentalizing system on the other hand has also been proposed to be crucial to infer intentions from observed actions (Van Overwalle, 2009; Van Overwalle and Baetens, 2009; Hamilton and Marsh, 2013; Spunt and Lieberman, 2013; Catmur, 2015; Begliomini *et al.*, 2017). Socially intended movements as well as imagined social interactions have been shown to lead to an activation in regions of both mirror neuron and mentalizing systems (Becchio *et al.*, 2012; Trapp *et al.*, 2014). Especially the posterior superior temporal sulcus (pSTS) – part of both systems- was suggested to be essential for the perception of social interactions, which provides the basis for social action understanding and interpretation (Isik *et al.*, 2017; Walbrin *et al.*, 2018). Besides the social content, the generation of predictions based on the communicative gesture might need more cognitive resources than in the individual condition. These differences in executive control and cognitive load could also lead to differences in prefrontal activation.

In the time segment (2) after the onset of agent B's response actions (or its replacement with noise dots), participants were able to validated their predictions in the

communicative condition and tried to detect a second agent in the cloud of (noise) dots in all conditions. Communicative actions in contrast to individual ones performed by the first agent were thought to increase the predictability of agent B's response action and should, thus, facilitate the detection of it (Manera, Becchio, *et al.*, 2011; von der Lühe *et al.*, 2016; Zillekens *et al.*, 2019). This could again lead to differences in the cognitive resources needed between conditions. Moreover, the predictability of agent B's action should lead to more motor system activation (Ulloa and Pineda, 2007; Pavlidou *et al.*, 2014; Palmer *et al.*, 2016; Braukmann *et al.*, 2017; Cheng *et al.*, 2017) in expected compared to non-expected outcomes.

In the time segment (3) before the participants' response, the participants had to decide whether the agent is actually present or absent. Inferring human actions from point-lights was shown to activate the motor system (Ulloa and Pineda, 2007; Perry *et al.*, 2010). The motor system might also be required to fill in the gaps between the point-light dots, so the single points are perceived as biological motion and thus a second agent rather than noise is seen (Saygin et al., 2004). Therefore, we expected pre- and post-central ROIs to be activated more in signal than in noise trials. In order to make the visual input comparable between conditions, signal and noise trails always contained the same number of dots, either constituting an agent B or moving in a random fashion. Moreover, we avoided confounding factors from incorrect responses by only analyzing trials with correct responses: Signal trials in our neural analyses, therefore, mean that agent B was present and was indeed correctly detected. Noise trials mean that agent B was not present and was also not erroneously detected.

Zillekens et al. (2019) did not only find differences between the communicative and individual condition in the BOLD signal in specific ROIs, but also in the functional coupling of ROIs with the amygdala. While EEG does not allow us to investigate the temporal dynamics in the amygdala, we were interested in the functional coupling between the cortical ROIs and how they differed across the communicative and individual conditions. Therefore, we performed exploratory coherence analyses with *a priori*-defined ROIs according to the study of Zillekens et al. (2019).

Behaviorally, we calculated two signal detection theory parameters to differentiate between the presence and absence of a second agent (i.e., the sensitivity) and to evaluate the tendency to choose presence or absence (i.e., the response criterion) (Stanislaw and Todorov, 1999). We expected that participants would perform better when point-light agents engage in communicative actions rather than in individual ones (expressed by enhanced sensitivity in communicative trials) and would be more likely to perceive a second agent after communicative than individual gestures (expressed by a decreased, i.e. less conservative,

response criterion in communicative trials) (cf. Manera, Becchio, *et al.*, 2011; Manera, del Giudice, *et al.*, 2011; Zillekens *et al.*, 2019). As these previous studies suggest that communicative gestures provide information to predict the other person's behavior and thus facilitate the perception of another agent, reaction times should be faster in communicative than in individual trials. Detecting an actually present agent B will result in an immediate response and thus signal trials are expected to result in faster reaction times than noise trials (with agent B being absent).

METHODS

Participants

An *a priori* power analysis was performed using G*power (Faul *et al.*, 2007) to determine the appropriate sample size. We used a power of 0.95 and an estimated effect size dz of 0.56 based on the behavioral study of Zillekens et al. (2019), which showed that participants achieved a higher performance in trials with communicative compared to individual actions using the same experimental design. The *a priori* power analysis suggested a sample size of 36 when using a one-tailed t-test for matched pairs and a significance level of 0.05. As artifacts are common in EEG studies, we recorded 15% more participants, resulting in a sample size of 41 volunteers. Using Mueller-Putz et al.'s (2008) formula as a basis, two participants were removed from all analyses, as their performance did not surpass chance level. The final sample consisted of 39 participants (21 female, 18 male) between the ages of 20 and 50 years (M = 25.62, SD = 6.37), all right-handed with normal or corrected to normal vision, no diagnosis of neurological or psychiatric disorders, and no history of medication intake. Additionally, Autism Spectrum Quotient values were indicative of a neuro-typical control group (M = 15.64, SD = 5.55) (Baron-Cohen *et al.*, 2001).
Flyers and circular emails were used to recruit volunteers at the Ludwig-Maximilians-Universität München. A monetary compensation of 10 € per hour was given to all participants for their time and effort. The study was approved by the ethics committee of the Faculty of Psychology and Education Sciences at Ludwig-Maximilians-Universität München and is in accordance with the guidelines of the Declaration of Helsinki. Some data from a sub-sample of the recorded participants has been published in relation to a research question not addressed in this manuscript (Friedrich et al., 2022).

Experimental Design

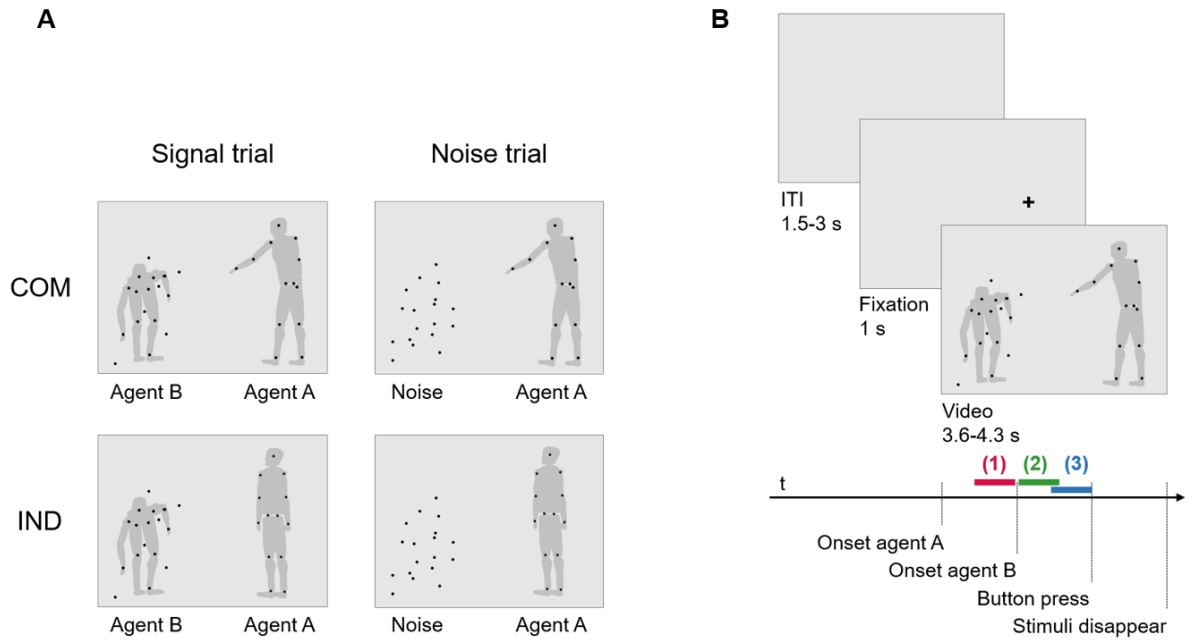

Figure 1. *Experimental design (adapted from Zillekens et al. (2019) and Friedrich et al. (2022)).* (A) Experimental conditions. Participants observed a screen with two point-light agents. Agent A either performed a communicative (COM, see top row) or an individual (IND, see bottom row) gesture. The responding Agent B was either present and masked in a cloud of noise dots (i.e., signal trial, see left column) or absent and entirely replaced by noise dots (i.e., noise trials, see right column). In this figure, we added grey silhouettes to make the agents visible, however, they were not displayed in the experimental task for the participants. (B) Structure of a trial. A trial consisted of a jittered inter-trial-interval between 1.5-3 s and a 1-s fixation cross indicating at which position agent A will appear next. Then the video with the two point-light agents started. Although both agents were present right from the video's onset, agent B's response action was delayed. The exact onset of agent B's goal-directed response action and the duration of the video varied between trials and was dependent on the actions performed. Participants were asked to first focus on agent A. Then they should observe the cloud of noise dots and decide by button press whether agent B was present or absent. We divided the video in three time segments for analyses. Time segment (1) before agent B's onset: Participants passively observed agent A performing either a communicative or individual action. Time segment (2) after agent B's onset: Participants watched the responding agent B, which was masked with noise dots or entirely replaced by noise dots. Time segment (3) before the response: Participants decided whether agent B was present or absent in the cloud of noise dots and indicated their choice with a button press.

The experimental design was controlled using the Psychophysics Toolbox (Version 3.0.14; Brainard 1997; Kleiner, Brainard, and Pelli 2007; Pelli 1997) in Matlab R2016a (The MathWorks, Inc., Natick, Massachusetts, United States) and was based on Zillekens et al.'s (2019) study.

Participants were facing a computer monitor (refresh rate = 60 Hz, resolution of 1280 x 1024) displaying black dots moving on a grey background (Figure 1). One half of the display contained moving dots that represented a well recognizable point-walker (agent A), executing either one of three communicative or one of three individual actions (communicative condition: asking to squat down, asking to look at the ceiling, asking to sit down; individual condition: turning around, sneezing, drinking). In 50 % of the trials, the other half of the display contained a second point-walker (agent B) within a cloud of spatially and temporally scrambled moving dots (signal trials: squatting down, looking at the ceiling, sitting down). In the remaining 50 % of trials, agent B was substituted by randomly moving noise dots (noise trials: agent B absent). Agent A's actions therefore determined if a trial belonged to the communicative or individual condition, whilst agent B's presence or absence defined a trial as a signal or noise trial (Figure 1A).

Trials began with the presentation of a blank screen for a jittered inter-trial-interval between 1.5 – 3 s, followed by a fixation cross for 1 s indicating if agent A would appear on the left or right half of the display (Figure 1B). Following this, the video depicting agent A simultaneously with the cloud of dots on the opposing side of the display (with or without the presence of agent B) was shown. Although the dots constituting agent B were visible from the beginning, the onset of agent B's response action was delayed. Agent B's response action was defined by a goal/spatially-directed dot movement exceeding a velocity of 10 angles/s for a minimal duration of 100ms (Ansuini *et al.*, 2015). The delay between the start of agent A's action and the start of agent B's action, ranged between 1267 – 1567ms and was dependent on the specific movement. The whole video had a duration ranging between 3600ms to 4300ms based on the particular action shown.

Participants were instructed to watch agent A first and only then attend to the cloud of dots. Following this, they were asked to press a button as swiftly as possible to indicate if agent B was present (signal) or absent (noise). Valid responses were required before the dots vanished. Using a standard German (QWERTZ) keyboard, response button assignment for yes and no (V- or N-key) was counterbalanced across participants. Furthermore, which point-walker appeared on the left or right side of the display was counterbalanced.

Analogous to the approach in Zillekens et al. (2019), the agents' actions were selected from the Communicative Interaction Database (Manera *et al.*, 2010). The actions were reliably identified as communicative or individual in their study (Manera *et al.*, 2010). The agents always faced each other and kept a comparable distance from the center. The

number of dots, the movement velocity as well as the onset an duration of the movements were kept stable between the communicative and individual conditions. In the communicative condition, agent B's response action matched the communicative action of agent A in timing, position and kinematics (Manera, del Giudice, *et al.*, 2011). In the individual condition, agent A's communicative movement was replaced by an individual action with an identical temporal onset and duration.

The dots constituting agent B were presented using a limited life-time technique: Thirteen possible dot locations defined agent B's body. However, at any given time only 6 of these possible locations comprised signal dots. Every 200ms, a dot would disappear and reappear at another location, with the timing of dot appearance being desynchronized. This limited lifetime technique was implemented to prevent participants from depending on the simultaneous transition of dots representing agent B's body. For more details, please see (Manera, del Giudice, *et al.*, 2011; Zillekens *et al.*, 2019).

Procedure and EEG Data Acquisition

All participants provided written informed consent, their age, gender, and completed the short form of the Edinburgh Handedness Inventory (Veale, 2014) in addition to the online version of the AQ (Autism Research Center; Baron-Cohen et al. 2001) prior to the EEG experiment. Moreover, the absence of neurological or psychiatric disorders, brain injuries, medication intake and pregnancy were all confirmed in a short telephone interview.

To record EEG during the experiment, 61 scalp electrodes (Ag/AgCl ring electrodes; Easycap ®) were placed following the international 10-10 system. Electrodes were applied on the right and left outer canthi and below the left eye to measure the electrooculogram (EOG). Fpz was used for the ground electrode and the reference was positioned on the nose tip. A sampling rate of 1000 Hz and a 64-channel amplifier system (BrainAmp, Brain Products ®) were used for signal acquisition, while impedances were maintained below 10 kΩ.

To ensure participants could achieve an average performance around 70% correct responses, an established procedure utilizing a pretest of 108 trials was employed to individually adapt the difficulty level (i.e., the number of noise dots masking agent B); participants had to press a button to signal if agent B was present or absent within a cloud of dots with alternating difficulty (i.e., a cloud of 5, 20 or 40 interfering dots). By fitting a cumulative Gaussian function to the performance of the participants the number of dots necessary for an accuracy of 70% was calculated. A minimum of five dots was used, regardless of if the calculated number of dots was lower (Manera, Becchio, *et al.*, 2011;

Manera, del Giudice, *et al.*, 2011; Zillekens *et al.*, 2019). The resulting number of noise dots for each individual participant was used to mask agent B in the main experiment.

Participants were given the opportunity to practice the experimental task during twelve practice trials. Following this, participants completed 288 experimental trials divided into four 9-min blocks with breaks included between blocks.

Behavioral Data Analyses

Behavioral data analyses were completed in Matlab R2016a, whereas statistical analyses were performed in IBM® SPSS® Statistics version 24.0.0.0 and JASP version 0.9.2 and 0.16.3 (JASP Team, 2019).

We defined the onset of agent B's response action at 1567 ms after the video onset for the action ‘sitting down’, 1500 ms for the action ‘squatting down’, and 1267 ms for the action ‘looking at ceiling’ (Figure 1B) (Ansuini *et al.*, 2015).

Trials in which a response was given prior to the onset of agent B plus 200 ms or after agent A and B had already disappeared were removed from the analysis. Reaction times (RTs) comprised the time window between the onset of agent B’s action and the button press (Figure 1B).

We calculated the hit rate (proportion of true positive responses of all signal trials) and the false alarm (FA) rate (proportion of false positive responses of all noise trials), z-transformed the rates and computed the two signal detection theory parameters sensitivity d’ and response criterion c as follows (Macmillan and Creelman, 1990; Zillekens *et al.*, 2019):

$d' = Z(Hit\ rate) - Z(FA\ rate)$ (1)

$c = -(1/2) * [Z(Hit\ rate) + Z(FA\ rate)]$ (2)

EEG Data Analyses

BrainVision Analyzer 2.0 (Brain Products ®) was employed to pre-process the EEG data. A preliminary visual inspection was conducted to remove large artifacts and interpolate bad channels. Out of the 61 EEG channels, 1 channel had to be interpolated for 3 participants, 2 channels for 2 participants and 3 and 5 channels each for one participant. Data was filtered between 0.1 and 120 Hz (48 db/oct), and a notch filter was applied at 50 Hz. Re-referencing of EOG channels was accomplished using a bipolar reference (i.e., right – left horizontal EOG channels, bottom vertical EOG channel – FP1), whereas a common average reference was utilized for the re-referencing of EEG channels. Blinks (vertical eye movements) and saccades (horizontal eye movements) were identified with an Independent Component Analysis for ocular correction on the bipolar EOG channels. Following the removal of

components clearly representing artifacts, a further visual inspection was conducted to identify and remove any remaining artifacts. To accommodate the sLORETA analyses data was re-sampled to 1024 Hz.

As the onset of agent B and the time point of participants' responses varied between trials, data cannot be averaged and analyzed over the entire time course. Instead, each trial was separated into three time segments in relation to these two events (Figure 1B):

(1) 1 s before agent B's onset (i.e., observation of agent A)
(2) 1 s after agent B's onset (i.e., observation of agent B)
(3) 1 s before the response (i.e., decision whether agent B is present or absent)

Solely trials in which a response was made 1 s after agent B had started moving and ahead of the stimuli disappearing were included. An average of 25 trials (SD= 23.4) of the total 288 per participant had to be discarded because the response occurred before 1 s. An average of 37 trials (SD= 24.8) had to be discarded because no response or a response occurred after the agents had disappeared. This left between 162 and 271 remaining trials of the 288 per participant. All analyzed trials are free of motor responses, while simultaneously containing a valid response. As the mean reaction time over participants and all trials was 1601 ms, time segment (2) and (3) overlapped on average about 400 ms.

Segments without artifacts were exported for the following contrasts:

(1) communicative (i.e., COM: agent A performs a communicative action) versus individual (i.e., IND: agent A performs an individual action) condition
(2) non-expected (i.e., trials in which a communicative action from agent A is followed by noise or an individual action from agent A is followed by the presence of agent B) versus expected outcome (i.e., trials in which a communicative action from agent A is followed by the presence of agent B or an individual action from Agent A is followed by noise).
(3) signal (i.e., agent B was present) versus noise (i.e., agent B was replaced by randomly moving noise dots) trials

EEG Amplitude analyses

The correct trials (i.e., hits and correct rejections) were further analyzed using Matlab R2015b and sLORETA v20190617 (Pascual-Marqui, 2002; Pascual-Marqui, 2007).
All 39 participants had ≥ 20 trials for each condition for the comparison of the contrasts communicative versus individual condition and signal versus noise trials. For the contrast of

non-expected versus expected outcome, 4 subjects had less than 20 trials for each condition, thus this contrast only included 35 participants.

The amplitude analysis comprised the computing of EEG crossspectra across all single trials, for each individual participant and condition, in the frequency range between 1-40 Hz, and the extraction of global field power. Subsequently, the scalp-level data was converted into voxel-based Standardized Low Resolution Electromagnetic Tomography (sLORETA) data (i.e., source space).

For the a priori ROI-based analyses, the data for each of the contrasts was extracted for the coordinates of the specific ROIs according to the study of Zillekens et al. (2019), which showed a significant difference in the BOLD signal within the three contrasts and were close enough to the cortical surface to be recorded with EEG (see Supplementary Tables S1-S3). For the data-driven whole brain analyses, this step was not necessary, as all voxel-based data entered the statistical analysis.

The statistical analyses for the a priori ROI-based and the data-driven whole brain data were performed over the (A) theta (4-7 Hz), (B) alpha (8-12 Hz), (C) lower beta (13-17 Hz), and (D) upper beta (18-25 Hz) frequency band for each of the three time segments: 1-s before and 1-s after agent B's onset and 1-s before the response. To compute a two-tailed t-statistic for paired groups the sLORETA built-in voxelwise randomization test (5000 permutations) was employed. This method to correct for multiple comparisons relies on statistical non-parametric mapping (SnPM) to calculate corrected critical thresholds and p values.

Exploratory coherence analyses based on a priori source-level ROIs for the communicative versus individual condition

We performed coherence analyses based on the *a priori*-defined ROIs according to the study of Zillekens et al. (2019) (Supplementary Table S4). These ROIs showed differences between the communicative and individual condition in their functional coupling to the amygdala. Here, we investigated differences between the communicative and individual condition in their functional coupling to each other.

For the coherence analyses, the preprocessing, the number of participants and the analyses tools were the same as for the EEG amplitude analyses. The figures were created using Fieldtrip (Tzourio-Mazoyer et al., 2002; Oostenveld et al., 2011). We also used the same minimum number of trials. However, for the coherence analysis, the number of trials between conditions was kept equal for each participant (as unequal numbers of trials across conditions can influence coherence values). This was done by randomly excluding trials until the lowest number of trials in any condition was matched. For each condition, EEG

crossspectra were computed over the remaining single trials in the frequency range between 1-40 Hz, separately for each subject and condition. Lagged coherence values (eliminating any spurious zero-phase lag coherence due to volume conduction) were extracted for the defined ROIs in source space according to Supplementary Tables S4. Coherence coefficients vary between 0 and 1. Two-tailed, paired t-statistics for theta, alpha, lower beta and upper beta frequency bands were computed for all possible ROI connections. Correction for multiple comparisons was applied using randomization tests the same way as done for the amplitude analysis.

RESULTS

Behavioral Results

As intended by the individual adjustment of difficulty, participants achieved a performance of 71.65% (*SD* = 8.66) correct responses at an average difficulty level of 13.05 (*SD* = 10.07; range 5 -44) interfering noise dots.

Normal distribution was not violated for the sensitivity (d'), thus a one-tailed paired-sample t-test was calculated to test the hypothesis of higher sensitivity d' in the communicative as compared to the individual condition. The increase in d' in the communicative (M = 1.32, SD = 0.61) compared to the individual condition (M = 1.29, SD = 0.64) remained non-significant ($t(38) = 0.38$, $p = .35$; *Cohen's d* = 0.061; Figure 2A).

The response criterion (c) was not normally distributed, thus a one-tailed Wilcoxon test was calculated. Confirming our hypothesis, c was lower in the communicative (M = -0.10, SD = 0.52) than in the individual condition (M = -0.04, SD = 0.49) ($Z = -1.66$, $p < .05$, *rank-biserial r* = -0.31; Figure 2B). Additionally, we tested whether there was a response bias in the individual and communicative conditions towards 'present' or 'absent' responses, reflecting a positive or negative deviation from zero. While a one-sample Wilcoxon test revealed no significant response bias in the individual condition ($Z = -0.81$, $p = 0.21$, *rank-biserial r* = -0.15), responses in the communicative condition were significantly biased towards reporting the presence of a second agent (i.e. tendency to press 'yes') ($Z = -1.73$, $p < 0.05$, *rank-biserial r* = -0.32, one-tailed).

To analyze reaction times, a 2 x 2 ANOVA was calculated with the factors communicative/individual condition and signal/noise trials. These were normally distributed. Confirming our hypothesis, responses occurred significantly faster in the communicative (M = 1601.42 ms, SD = 193.25 ms) than in the individual condition (M = 1622.90 ms, SD = 183.99 ms) ($F(1,38) = 5.91$, $p < 0.05$, *partial* $\eta^2 = 0.14$) and faster for signal (M = 1586.12 ms, SD =

169.41 ms) than for noise trials (*M* = 1637.88 ms, *SD* = 198.01 ms; $F(1,38) = 4.28$, $p < 0.05$, *partial* $\eta^2 = 0.10$ (Figure 2C). There was no interaction of experimental factors ($F(1,38) = 0.08$, $p = 0.76$, partial $\eta^2 = 0.00$).

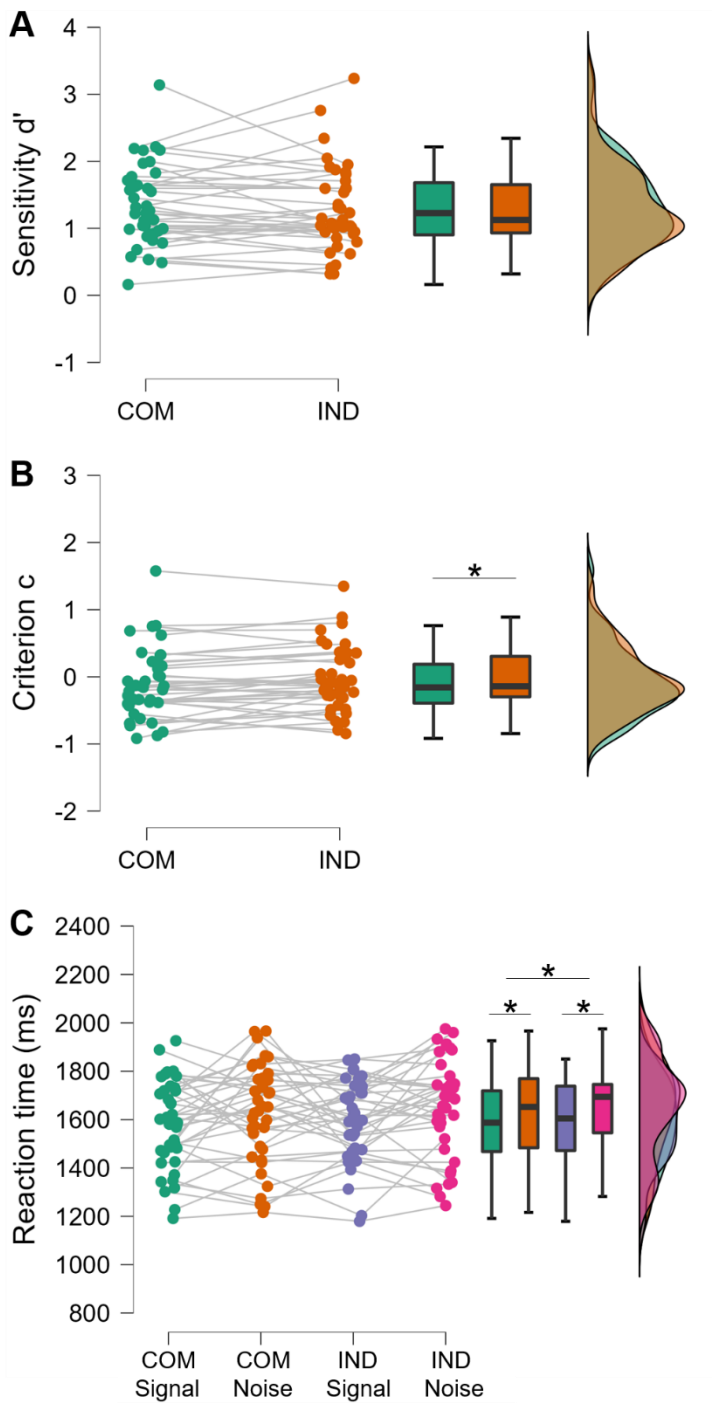

Figure 2. *Behavioral results.* (A) Mean sensitivity d' values and (B) mean criterion c values in the communicative (COM) and individual (IND) conditions. (C) Mean reaction times in ms for signal and noise trials separately for the communicative and individual condition. The raincloud plots show first the individual data points, then box plots and last the distribution of the data. Statistically significant differences are indicated with an asterisk ($p < 0.05$).

EEG Results

Contrast of the communicative versus individual condition

A priori ROI-based Amplitude Analyses

This contrast was computed for the 20 ROIs (see Supplementary Table S1), which showed a significant difference in the BOLD signal for the contrast communicative versus individual condition in the study of Zillekens et al. (2019). We could not find significant differences in the EEG amplitude analyses in the 20 ROIs in any frequency band and time segment (Table 1A).

Data-Driven Whole Brain Amplitude Analyses

In the time segment (1) before agent B's onset, significantly higher theta (4-7 Hz) amplitude was shown in the communicative than individual condition in the left middle frontal gyrus ($p < 0.05$, see Table 1A in bold letters for statistical parameters and coordinates and Figure 3A).

Contrast of the non-expected versus expected outcome

A priori ROI-based Amplitude Analyses

This contrast was tested within the 5 ROIs (see Supplementary Table S2), which showed a significant difference in the BOLD signal for the contrast non-expected (communicative noise trials and individual signal trials) versus expected (communicative signal trials and individual noise trials) outcome in the study of Zillekens et al. (2019).

In the time segment (2) after agent B's onset, significantly higher amplitude in the lower beta (13-17 Hz) frequency band (i.e., lower beta desynchronization/ lower activation) was shown in the non-expected compared to the expected outcome at the right posterior medial frontal gyrus ($p < 0.05$, see Table 1B written in normal black letters and Figure 3B).

Data-Driven Whole Brain Amplitude Analyses

No significant results were found (Table 1B).

Contrast of signal versus noise trials

A priori ROI-based Amplitude Analyses

This analysis was computed for the 18 ROIs (see Supplementary Table S3), which showed a significant difference in the BOLD signal for the contrast signal versus noise trials in the study of Zillekens et al. (2019).

In the time segment (3) before the response, the signal trials showed significantly lower beta amplitude (i.e., more desynchronization/ more activation) than the noise trials in the lower frequency range (13-17 Hz) at the left cuneus und the left calcarine gyrus and in the upper frequency range (18-25 Hz) at the left precuneus ($p < 0.05$, see Table 1C written in normal black letters and Figure 3C).

Data-Driven Whole Brain Amplitude Analyses

In the time segment (3) before the response, the effect in the beta frequency band in the precuneus und cuneus was confirmed ($p < 0.05$, see Table 1C in bold letters and Figure 3C). Additionally, in the same time segment (3), the signal trials showed significantly lower amplitude in the theta and alpha frequency band at the left superior temporal gyrus ($p < 0.05$, see Table 1C and Figure 3C). In the alpha frequency band, the significant effect was stronger than in the theta band and spread to the middle temporal gyrus, the Inferior temporal gyrus, the supramarginal gyrus, the inferior parietal lobule, the parahippocampal gyrus, the lingual gyrus and the fusiform gyrus (see Figure 3C and Figure S3 A and B).

Table 1. *Statistical results of the EEG amplitude analyses.* The rows depict the contrasts divided in the five frequency bands and the columns the three time segments. All indicated results are significant on the 5% alpha level ($p < 0.05$) and include the t value, the effect size dz and the region, the Brodmann area (BA) and the coordinates according to the Montreal Neurological Institute (MNI) template (x/y/z) for the most significant voxel. The results from the *a priori* ROI-based analyses are written in normal black letters, the results from the data-driven whole brain analyses are written in bold and all results that are illustrated in Figure 3 are highlighted in grey.

At the indicated regions in specific frequency bands and time segments, the table indicates (A) a significant amplitude increase in the communicative (COM) in comparison to the individual (IND) condition (number of participants (N) = 39), (B) a significant amplitude increase in the non-expected (Non-exp) than expected (Exp) outcome (N=35) and (C) a significant amplitude decrease in signal in comparison to noise trials (N= 39). In time segment (1) before agent B's onset (i.e., observation of agent A), it is yet impossible to differentiate between signal and noise or non-expected and expected outcome (both dependent on agent B), thus only the contrast COM vs. IND (related to agent A) was computed for this time segment. All effects in other time segments and frequency bands remained non-significant (n.s.).

	Time segment (1) before agent B's onset	Time segment (2) after agent B's onset	Time segment (3) before the response
(A) COM > IND (N = 39)			
Theta	**t = 3.69, dz = 0.59 L Middle Frontal Gyrus (BA 10), -45/50/5**	n.s.	n.s.
Alpha	n.s.	n.s.	n.s.
Lower beta	n.s.	n.s.	n.s.
Upper beta	n.s.	n.s.	n.s.
(B) Non-exp > Exp (N = 35)			
Theta	-	n.s.	n.s.
Alpha	-	n.s.	n.s.
Lower beta	-	t = 2.75, dz = 0.46 R Posterior Medial Frontal Gyrus (BA 6), 10/-18/64	n.s.
Upper beta	-	n.s.	n.s.
(C) Signal < noise (N = 39)			
Theta	-	n.s.	**t = -3.70, dz = 0.59 L Superior Temporal Gyrus (BA 22), -60/-30/5**
Alpha	-	n.s.	**t = -4.02, dz = 0.64 L Superior Temporal Gyrus (BA 13), -50/-45/20**
Lower beta	-	n.s.	**t = -4.15, dz = 0.66 Bilateral Cunei (BA 18), -15/-80/25** t = - 4.06, dz = 0.65 L Cuneus (BA 18), -10/-86/28 t = -3.74, dz = 0.60 L Calcarine Gyrus (BA 18), -2/-82/20
Upper beta	-	n.s.	**t = -3.76, dz = 0.60 Bilateral Precunei (BA 7), 0/-60/35** t = -3.37, dz = 0.54 L Precuneus (BA 7), -8/-50/52

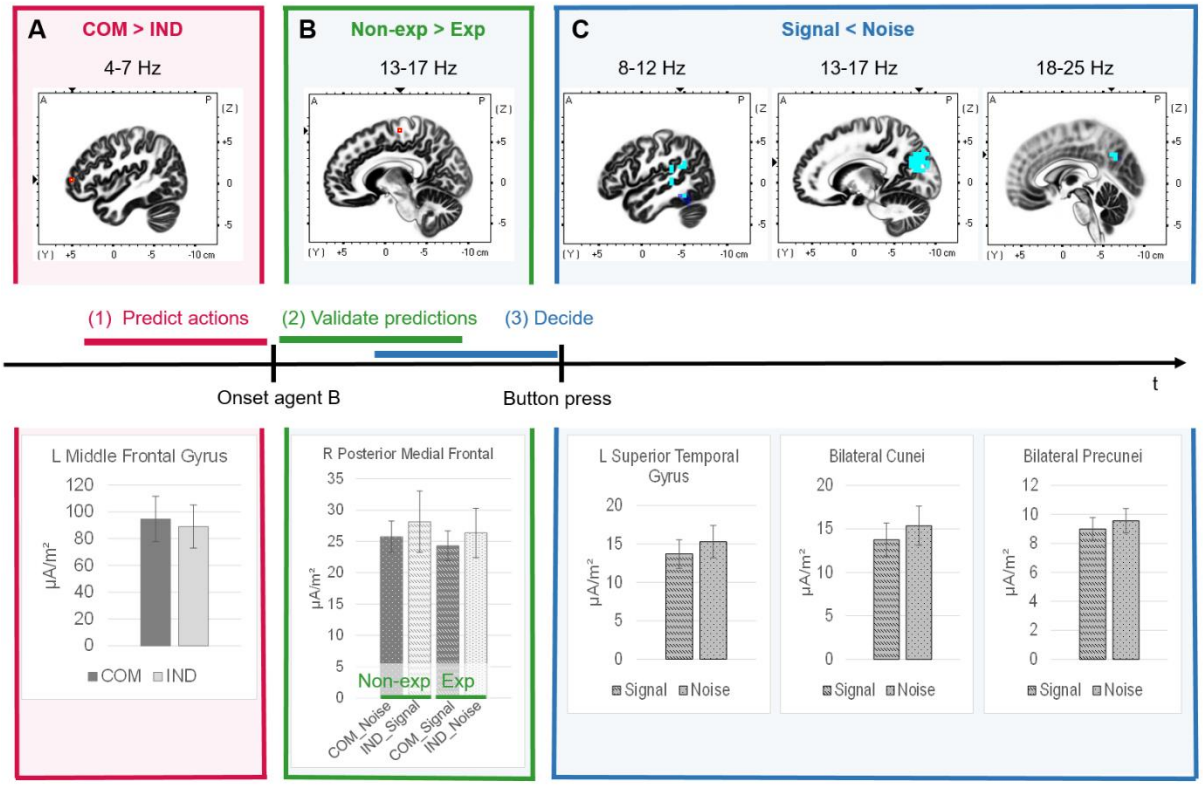

Figure 3. *Brain patterns of significant amplitude changes.* The top row depicts the voxels in the sagittal brain view, which show significant amplitude changes. Turquoise/blue colors indicate an amplitude decrease and yellow/red colors indicate an amplitude increase. The bottom row shows bar graphs indicating the mean amplitude +/- standard error of the mean at the voxel with the most significant difference indicated in the brain maps above. (A) In the time segment (1) before agent B's onset, higher amplitude was shown in the theta band in the communicative (COM) than in the individual (IND) condition in the left Middle Frontal Gyrus (Brodmann area (BA) 10) with the peak difference at the MNI coordinates-45/50/5 (red section; for additional brain views see Figure S1). (B) In the time segment (2) after agent B's onset, higher amplitude was shown in the lower beta band in the non-expected (Non-exp) than in the expected (exp) outcome in the right Posterior Medial Frontal Gyrus (BA 6) with the a priori defined MNI coordinates 10/-18/64 (Zillekens *et al.*, 2019) (green section; for additional brain views see Figure S2). (C) In the time segment (3) before the response, lower amplitude was shown in the signal compared to the noise trials. This difference was significant in the L Superior Temporal Gyrus in the theta (for a graphical illustration, please refer to Figure S3 A) but mainly in the alpha frequency band (left side of the blue section; for additional brain views see Figure S3 B). In the alpha frequency band, the most significant voxel was in the superior temporal gyrus in BA 13 (MNI: -50/-45/20) but there were also significant voxels in B 41 in the superior temporal gyrus. Additionally, the middle temporal gyrus (BA 21 and 22) and the Inferior temporal gyrus (BA 20), the Supramarginal gyrus

(temporal lobe, BA 40) as well as the inferior parietal lobule (parietal lobule, BA 40), the parahippocampal gyrus (BA 19, 27, 28, 30, 35 and 36), the lingual gyrus (BA 18, 19) and the fusiform gyrus (temporal and occipital lobe, BA 37) showed significantly lower alpha amplitude in the signal compared to noise. In the lower beta band, this difference showed peak significance in the Bilateral Cunei (BA 18; MNI: -15/-80/25; middle of the blue section; for additional brain views see Figure S3 C). This significant effect also spread to BA 7 and 19 of the Cuneus (occipital lobe) and to the Precuneus (parietal lobe, BA 31). In the *a priori* ROI-based analysis, the significant amplitude decrease in the signal compared to noise trials in the left Cuneus (BA18) was confirmed and additionally found in the left Calcarine Gyrus (BA 18) (for a graphical illustration, please refer to Figure S4 A and B). In the upper beta band, lower amplitude in the signal compared to noise trials was found in the Bilateral Precunei (parietal lobule, BA 7; MNI: 0/-60/35) (right of the blue section; for additional brain views see Figure S3 D). This significant difference spread slightly to the adjacent cingulate gyrus (BA 31) and was confirmed by the *a priori* ROI-based analysis (for a graphical illustration, please refer to Figure S4 C).

Exploratory coherence analyses based on a priori source-level ROIs for the communicative versus individual condition

The coherence analysis was computed for the 19 ROIs (see Supplementary Table S4), which showed a significant difference between the communicative and individual condition in the functional coupling to the amygdala in the study of Zillekens et al. (2019).
In the time segment (2) after agent B's onset, we found significantly lower coherence in the communicative than the individual condition in the lower beta band (13-17 Hz) between the left superior temporal gyrus and the right middle occipital gyrus ($t = -4.83$, $N = 39$, $p < 0.05$, $dz = 0.77$, see Figure 4).

Additionally, a trend emerged in the time segment (1) before agent B's onset: We found marginally higher coherence in the communicative compared to the individual conditions in the alpha band (8-12 Hz) between the left superior orbital gyrus and the right anterior cingulate cortex ($t = 4.20$, $N = 39$, $p < 0.1$, $dz = 0.67$, see Figure 4).

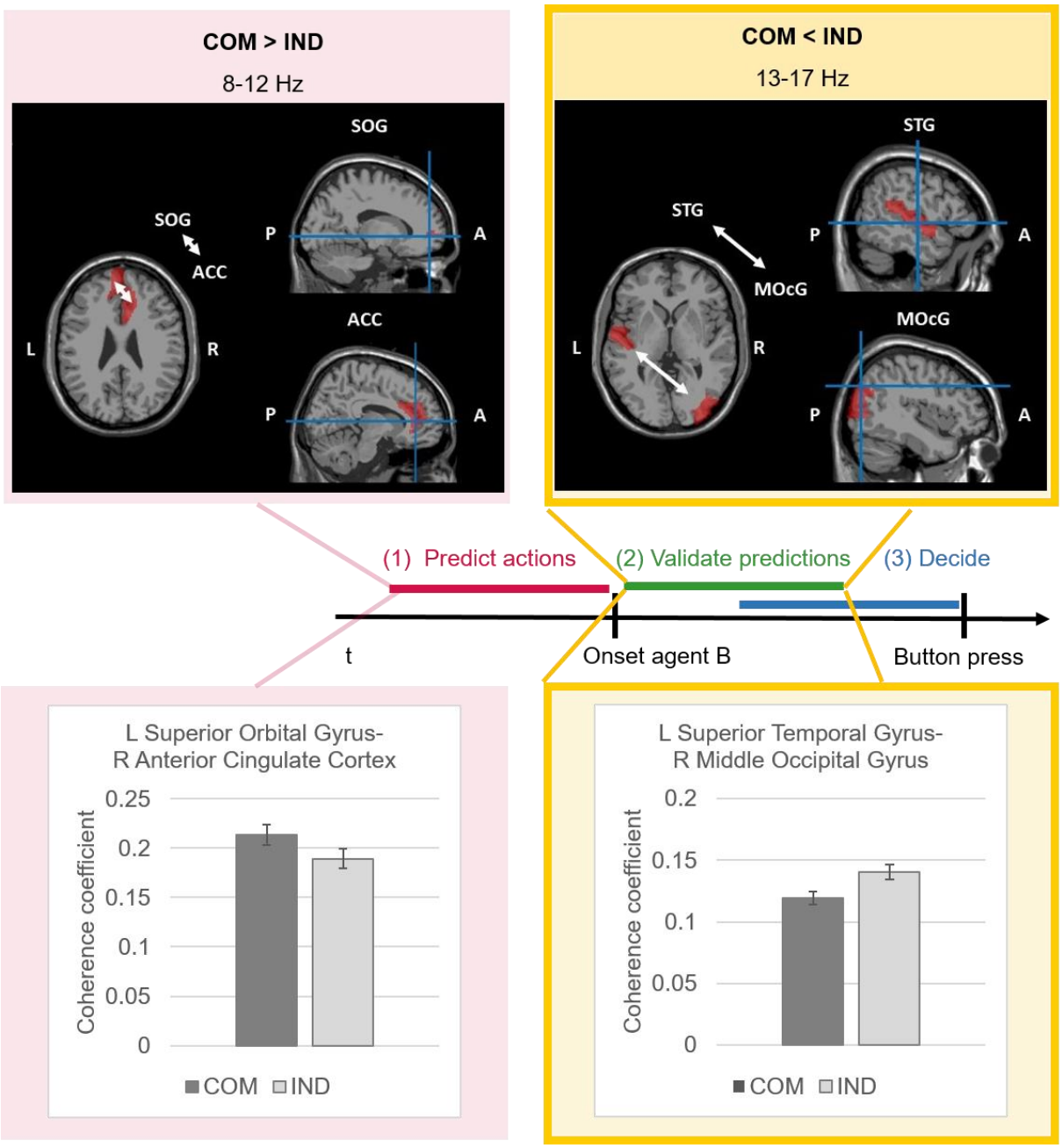

Figure 4. *Brain patterns of the coherence analyses.* The top row depicts the brain regions (indicated in red), in which the MNI coordinates of the *a priori*-defined ROIs fall that show significant lagged coherence. Slices on the left side of each panel are horizontal slices (L = left, R = right), those on the right side are sagittal slices (P = posterior, A = anterior) with the exact coordinates marked with a blue cross.

The bottom row shows bar graphs indicating the mean coherence coefficient +/- standard error of the mean between the two voxels indicated in the brain maps above. Yellow section: In the time segment (2) after agent B's onset, significantly lower beta coherence was shown between the left superior temporal gyrus (STG; -52/-14/0) and the right middle occipital gyrus (MOcG; 42/-78/34) in the communicative (COM) as compared to the individual (IND)

condition ($p < 0.05$). Additionally a trend is illustrated in the red section without a frame: In the time segment (1) before agent B's onset, higher alpha coherence between the left superior orbital gyrus (SOG; -16/52/-2) and the right anterior cingulate cortex (ACC; 10/38/6) was found in the communicative (COM) as compared to the individual (IND) condition by trend ($p < 0.1$).

DISCUSSION

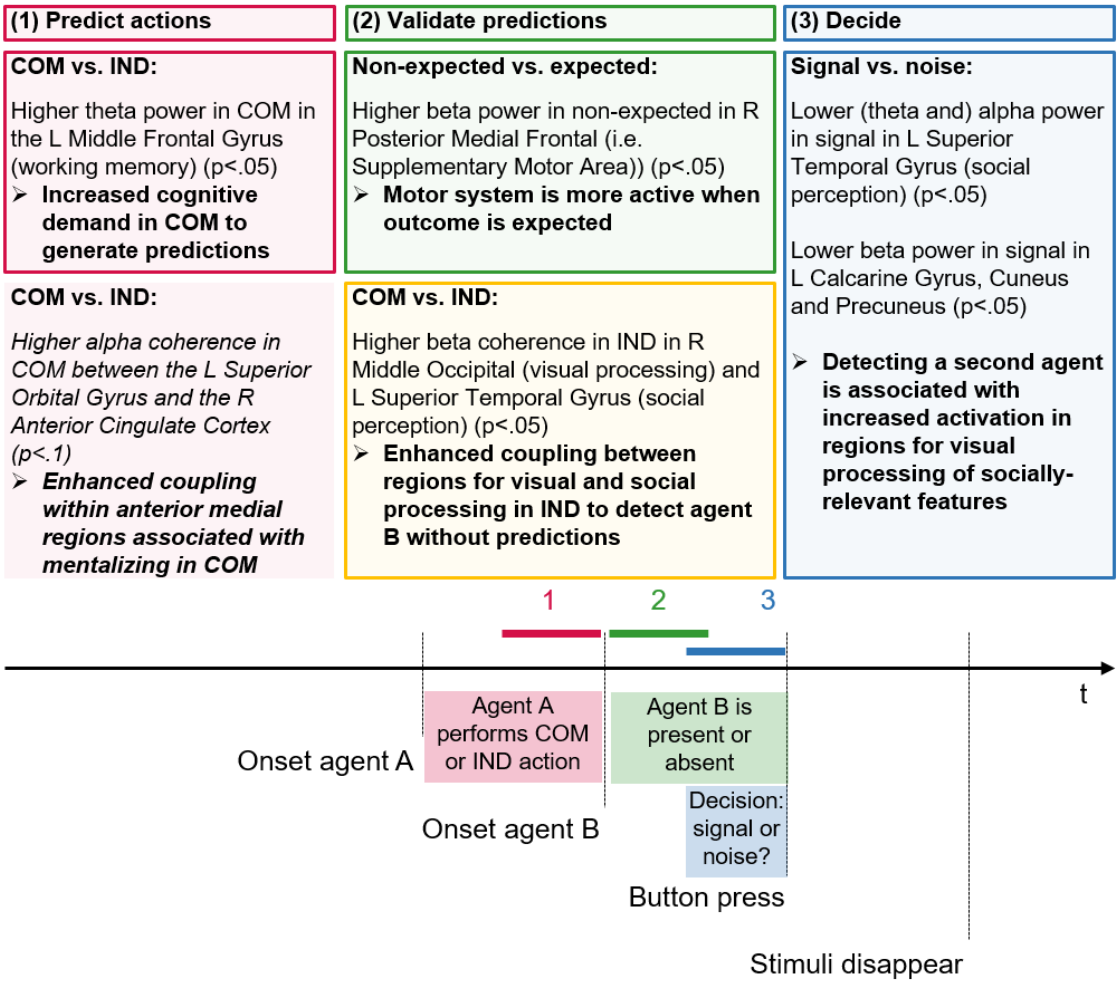

Figure 5. *Temporal dynamics of brain activity for interpersonal predictive coding.* The significant results and their interpretation (in bold) are summarized in the text boxes for the time segments (1) before agent B's onset (red sections), (2) after agent B's onset (green and yellow sections) and (3) before the response (blue sections). The results from the amplitude analyses are indicated in the *top* row in the red, green and blue frames. The results from the coherence analyses for the communicative (COM) versus individual (IND) condition are indicated in the *bottom* row in red without a frame (only trend) for time segment (1) and in yellow for time segment (2).

The aim of this study was to investigate the temporal dynamics of oscillatory brain activity during interpersonal predictive coding, i.e. when we perceive and predict actions from nonverbal cues in point-light displays and use them to detect the presence of a second agent to whom the behavior has been directed. We expected different brain networks to be involved during the formation of predictions, the validation of the predictions and the actual detection of the second agent.

The age, gender and AQ distribution of our sample was comparable to the preceding fMRI study by Zillekens et al. (2019). Using the same experimental design, the behavioral performance was similar across Zillekens' and the present study.

Confirming our hypothesis, participants were more biased towards reporting the presence of a second agent (i.e., adopted a less conservative response strategy) after observing a communicative as compared to an individual gesture of a first agent (Manera, del Giudice, *et al.*, 2011; Zillekens *et al.*, 2019). In contrast to our hypotheses, the finding of increased sensitivity (d') remained statistically non-significant when compared between the communicative and individual condition. Interestingly, Zillekens et al. (2019) could show a significant difference in in the sensitivity between the communicative and individual condition in their sample of the behavioral experiment, but this difference also remained non-significant in their fMRI experiment. We could confirm our hypotheses that responses occurred faster in the communicative than in the individual condition and faster for signal than for noise trials.

On the neural level, we found different brain regions to be active during different stages of the social interaction task (see Figure 5):

For the time segment (1) before agent B's onset, the data-driven whole brain analysis revealed that the communicative condition showed significantly higher theta amplitude than the individual condition in the left middle frontal gyrus (Table 1, Figure 3 and 5). The coordinates fall into the left dorsolateral prefrontal cortex area of the gyrus. A theta increase in the dorsolateral prefrontal cortex has been associated with working memory control processes (Wager and Smith, 2003; Sauseng *et al.*, 2004; Sauseng *et al.*, 2005; Sauseng *et al.*, 2010; Meyer *et al.*, 2015). This might indicate that the communicative condition recruited more working memory resources than the individual one as participants were forming predictions for agent B's response action.

In contrast to our hypotheses, our EEG amplitude analyses did not show higher activation in the communicative compared to the individual condition of regions engaged in mirror neuron activity and mentalizing. Neither was increased activation demonstrated in any temporal (Isik *et al.*, 2017; Walbrin *et al.*, 2018) or prefrontal networks previously associated with in social interaction processing (Sliwa and Freiwald, 2017). Zillekens et al. (2019) did not find activation of these regions when contrasting the communicative versus individual

conditions either. One explanation is that both conditions were perceived in terms of social biological motion as they included point-light displays showing moving agents (Zillekens *et al.*, 2019). In another recent publication from our lab, we have demonstrated higher sensorimotor activation in time segment (1) in false alarm compared to correct rejection and hit trials within the communicative condition (Friedrich *et al.*, 2022). We had interpreted this sensorimotor activation as a neural signature of generating predictions that outweigh sensory information presented later in the time segment (3) and thus leading to the illusion of seeing agent B (i.e., to seeing a Bayesian ghost). The fact that we did not find a difference in sensorimotor activation between the individual and communicative condition in the current data indicates that this sensorimotor activation is not related to generating predictions generally (which is possible in the communicative but not in the individual condition), but to generating top-down predictions that outweigh the bottom-up sensory information and thus lead to perceive a Bayesian ghost.

Although no amplitude differences were found between the communicative and individual conditions, a statistical trend emerged in the exploratory coherence analyses, which corroborates the results of Zillekens et al. (2019). Zillekens and colleagues (2019) had found that the amygdala was functionally coupled to the medial prefrontal cortex in communicative trials, whereas it increased its functional connectivity with fronto-parietal areas in the individual condition. Here, EEG coherence analyses between the cortical regions (note, that in the EEG no signal from the amygdala could be captured) revealed higher alpha coherence between superior orbital gyrus and the anterior cingulate cortex in the communicative compared to the individual condition during the observation of agent A (Figure 4 and 5). Both of these medial anterior regions are important for social tasks and might be involved in mentalizing processes (Amodio and Frith, 2006; Monticelli *et al.*, 2021). This means that the observation of communicative gestures and the resulting inference of actions in the time segment before the onset of agent B, may not only have led to the recruitment of more cognitive resources, but also to enhanced coupling and thus to a more efficient network within medial anterior regions associated with social and mentalizing processes.

In the time segment (2) after agent B's onset, participants could validate their predictions and try to detect agent B in a cloud of noise dots. Indicating the higher difficulty level of detecting a second agent without expectations about the specific movement, enhanced coupling between the middle occipital and the superior temporal gyrus was shown in the individual compared to the communicative condition (Figure 4 and 5). It has been shown that the visual system is sensitive to point-light biological motion (Pavlova, 2012). The superior temporal gyrus (STG) is a region involved in social perception and cognition (Baron-Cohen *et al.*, 1999; Jou *et al.*, 2010). The STG is strongly connected to the adjacent posterior

superior temporal sulcus (pSTS), a brain region part of the MNS and mentalizing system (Rizzolatti *et al.*, 2001; Schilbach *et al.*, 2013; Yang *et al.*, 2015). Thus, it has been associated with biological motion perception and social interaction (Caspers *et al.*, 2010; Pavlova, 2012; Isik *et al.*, 2017; Walbrin *et al.*, 2018). Moreover, Quadflieg and colleagues (2015) showed that both the left and right pSTS were more active in incongruent interactions (i.e., two persons performing non-matching individual actions) in comparison to congruent ones (i.e., two people performing a communicative action) (Quadflieg *et al.*, 2015), which is in line with our results.

In the time segment (2) after agent B's onset, we had furthermore assumed that the better predictability of an expected outcome leads to increased motor-relevant cortex activation as compared to a non-expected outcome (Braukmann *et al.*, 2017). Indeed, we found lower beta amplitude (i.e., beta suppression) in the expected outcome in comparison to the non-expected outcome after agent B's onset in the right posterior medial frontal gyrus (Table 1, Figure 3 and 5). The posterior medial frontal gyrus includes Brodmann Area 6, which consists of the premotor and supplementary motor area. The coordinates of the ROI in our analysis fall into the supplementary motor area (Tzourio-Mazoyer *et al.*, 2002; Kim *et al.*, 2010) (see Figure 3). As beta suppression over motor areas reflects motor-relevant activation (McFarland *et al.*, 2000), we here show evidence in favor of our hypothesis.

In contrast to our results, Zillekens et al. (2019) reported a higher BOLD response (i.e., more activation) for the non-expected than the expected outcome in the right posterior medial frontal gyrus together with the left cerebellum, left fusiform gyrus and parietal areas. This effect has been interpreted as being associated with the computation of error signals and the different processing of incongruent and congruent stimuli (Zillekens *et al.*, 2019). It seems that this motor-relevant brain area can be activated in both cases: first, during the processing of predictable actions and goal-directed movements (Ulloa and Pineda, 2007; Perry *et al.*, 2010; Braukmann *et al.*, 2017; Cheng *et al.*, 2017) and second, during the processing of errors (i.e., rather unpredictable or distorted movements) (Pavlidou *et al.*, 2014; Meyer *et al.*, 2016).

In the time segment (3) before the response, the decision had to be made whether to press 'yes' or 'no' and thus indicate whether agent B was present or absent. The number of dots displayed were kept stable over signal and noise trials. While we found a significant main effect of signal versus noise trials before the response, this difference did not become significant in the motor system as hypothesized. We found more activation (i.e., lower alpha and beta amplitude) in signal than noise trials in the occipital lobe, in the cuneus, the calcarine sulcus and the lingual gyrus which are involved in visual processing (Flores, 2002). Additionally, the temporal lobe was more activated in signal than noise trials: The superior temporal gyrus showed a strong effect in the alpha band with a marginal effect also in the

theta band, which was probably driven by alpha smearing into lower frequency bands. As already mentioned above, the superior temporal gyrus is a region involved in social perception and cognition (Baron-Cohen *et al.*, 1999; Jou *et al.*, 2010) and its adjacent pSTS is associated with social interaction processing (Isik *et al.*, 2017; Walbrin *et al.*, 2018). Moreover, we found more alpha decrease (i.e., more activation) in the middle temporal gyrus, the inferior temporal gyrus, the fusiform gyrus and the parahippocampal gyrus in signal than noise trials. The temporal gyrus is part of the ventral stream of visual processing and involved in object recognition (Kravitz *et al.*, 2014). The fusiform gyrus is specific to face recognition (Kanwisher *et al.*, 1997), whereas the parahippocampal gyrus is engaged in visual recognition of scenes (Epstein and Kanwisher, 1998).

The fact that the differences in the occipitotemporal regions remained non-significant between the communicative and individual condition but became significant for the comparison of signal and noise trials in this time segment before the response might be explained by the recent work of Wurm and Caramazza (2019). They suggested that the activation of the occipitotemporal regions is rather associated with visual processing of socially-relevant features such as the presence of a person, the directedness of actions or orientation of agents than an abstract representation of sociality (Wurm and Caramazza, 2019). In the present study, it seems that these regions are more sensitive to whether there is actually a second agent that can be perceived (i.e., presence/absence of the second agent) than whether the two agents interact with each other or not (communicative versus individual condition). These results also highlight the importance to look at different time segments and thus entangle the different cognitive processes involved in social tasks.

In the parietal lobe, we found more alpha decrease (i.e., more activation) in signal than noise trials in Brodman Area 40 of the supramarginal gyrus and the inferior parietal lobule. In the precuneus, there was an amplitude decrease in signal compared to noise trials in the beta band in the present study. While the Brodmann Area 40 was shown to be activated during mirror-like processing of action observation (Del Vecchio *et al.*, 2020), the precuneus is part of the mentalizing system (Van Overwalle and Baetens, 2009). Among others, the precuneus is involved in motor and mental imagery, processing of visuo-spatial information and attention as well as processing and understanding intentions and actions (Cavanna and Trimble, 2006; Schilbach *et al.*, 2006; Schilbach *et al.*, 2008; Schilbach *et al.*, 2012; Brandi *et al.*, 2021). As the effects in alpha and beta bands in the precuneus, cuneus and calcarine gyrus did not replicate the results from Zillekens et al. (2019), the results in the present study might represent a very specific activation right before the response is given. Contrary to analyzing the activation over the entire video duration, the strength of the current approach using EEG was to disentangle the specific cognitive processes involved in this complex task.

Taken together, in the time segment (3) before the response, signal compared to noise trials led to increased activation in regions relevant for visual processing, social perception and cognition rather than in the predicted motor areas. It seems that activation of the sensorimotor cortex is specific to perceiving a biological motion (or illusion) after a communicative gesture (Friedrich *et al.*, 2022). In the present study, we contrasted correct signal (i.e., hit) versus correct noise (i.e., correct rejection) trials collapsed over the communicative and individual condition. Our findings suggest that detecting a second agent correctly (i.e., providing the basis for a social interaction independently whether it follows a communicative or individual gesture) is associated with increased activation of regions involved in visual processing of socially-relevant features.

Conclusions

In this study, we demonstrated the neural temporal dynamics of perceiving and predicting actions from nonverbal social cues and of using them to optimize response behavior by means of EEG. First, the perception of communicative actions and the resulting predictions led to an enhanced functional coupling within medial anterior regions involved in social and mentalizing processes and a higher deployment of cognitive resources than required in the individual condition. Second, the detection of a social agent without the help of action predictions, led to enhanced coupling between regions for social perception and visual processing in the individual condition. In line with our hypothesis, an expected outcome was associated with increased activation of the motor system. Third, the correct detection of a second agent was associated with increased activation in areas for visual processing and social cognition rather than the predicted motor areas. Overall, our results confirm that different neural markers associated with different cognitive processes are dominant at different stages of social interactions and that it is crucial to consider the temporal dynamics during social interactions and their neural correlates.

Future studies could be extended to include individuals with social interaction difficulties or ‘disorders of social interaction’ (Schilbach, 2016) to investigate whether they show aberrant brain activity in the dynamic brain patterns described in this study. This would allow conclusions about which processes (cognitive, motor, visual or social) and stages (formation of predictions, validation of predictions, decision processes) are affected and may contribute to interactional problems. Here, an interesting avenue could be the use of brain stimulation techniques or neurofeedback training (Pineda *et al.*, 2008; Pineda *et al.*, 2014; Friedrich *et al.*, 2015; Nitsche and Paulus, 2011; Herrmann *et al.*, 2013; Amatachaya, 2014), to improve social interaction .

Acknowledgements

We would like to thank Cristina Becchio and Atesh Koul for providing the experimental task and advice during setup and analysis.

This study was funded by grants from the Deutsche Forschungsgemeinschaft (DFG) to EVCF (FR 3961/1-1) and to PS (SA 1782/2-2) and by the Max Planck Society via a grant for an independent Max Planck Research Group to LS.

Authors contributions

Conceptualization, E.V.C.F., I.C.Z., L.S., and P.S.; Methodology, E.V.C.F., I.C.Z., and P.S.; Software, E.V.C.F., A.L.B.; Validation, E.V.C.F., I.C.Z., A.L.B., and P.S.; Formal Analysis, E.V.C.F., I.C.Z., A.L.B., D.O., E.V.S., and J.S.; Investigation, E.V.C.F., D.O., and E.V.S.; Data Curation, E.V.C.F., A.L.B., D.O., E.V.S., and J.S.; Resources, P.S.; Writing – Original Draft, E.V.C.F., D.O., L.S., and P.S.; Writing – Review & Editing, E.V.C.F., I.C.Z., A.L.B., D.O., E.V.S., J.S., L.S., AND P.S.; Visualization, E.V.C.F. J.S.; Supervision, L.S. and P.S.; Project Administration, E.V.C.F., L.S., and P.S.; Funding Acquisition, E.V.C.F., L.S., and P.S.

Data availability statement

All the data associated with this manuscript will be made publicly available.

Declaration of interests

The authors declare no competing interests.

Bibliography

Amatachaya, A. (2014). Effect of anodal transcranial direct current stimulation on autism: a randomized double-blind crossover trial. *Behavioural Neurology*, **2014**, 173073

Amodio, D.M., Frith, C.D. (2006). Meeting of minds: The medial frontal cortex and social cognition. *Nature Reviews Neuroscience*, **7**, 268–77

Ansuini, C., Cavallo, A., Koul, A., et al. (2015). Predicting object size from hand kinematics: A temporal perspective. *PLoS ONE*, **10**, 1–13

Baron-Cohen, S., Ring, H.A., Wheelwright, S., et al. (1999). Social intelligence in the normal and autistic brain: An fMRI study. *European Journal of Neuroscience*, **11**, 1891–98

Baron-Cohen, S., Wheelwright, S., Skinner, R., et al. (2001). The Autism Spectrum Quotient : Evidence from Asperger syndrome/high functioning autism, males and females, scientists and mathematicians. *Journal of Autism and Developmental Disorders*, **31**, 5–17

Becchio, C., Cavallo, A., Begliomini, C., et al. (2012). Social grasping: From mirroring to mentalizing. *NeuroImage*, **61**, 240–48

Begliomini, C., Cavallo, A., Manera, V., et al. (2017). Potential for social involvement modulates activity within the mirror and the mentalizing systems. *Scientific Reports*, **7**, 1–9

Brainard, D.H. (1997). The Psychophysics Toolbox. *Spatial Vision*, **10**, 433–36

Brandi, M.L., Lahnakoski, J.M., Kopf-Beck, J., et al. (2021). Imagery of negative interpersonal experiences influence the neural mechanisms of social interaction. *Neuropsychologia*, **160**

Braukmann, R., Bekkering, H., Hidding, M., et al. (2017). Predictability of action sub-steps modulates motor system activation during the observation of goal-directed actions. *Neuropsychologia*, **103**, 44–53

Caspers, S., Zilles, K., Laird, A.R., et al. (2010). ALE meta-analysis of action observation and imitation in the human brain. *NeuroImage*, **50**, 1148–67

Catmur, C. (2015). Understanding intentions from actions: Direct perception, inference, and the roles of mirror and mentalizing systems. *Consciousness and Cognition*, **36**, 426–33

Cavanna, A.E., Trimble, M.R. (2006). The precuneus: A review of its functional anatomy and behavioural correlates. *Brain*, **129**, 564–83

Cheng, C.H., Sun, H.H., Weng, J.Q., et al. (2017). Differential motor cortex excitability during observation of normal and abnormal goal-directed movement patterns. *Neuroscience Research*, **123**, 36–42

Epstein, R., Kanwisher, N. (1998). The parahippocampal place area: A cortical representation of the local visual environment. *Nature*, **392**, 598–601

Faul, F., Erdfelder, E., Lang, A.-G., et al. (2007). G * Power 3 : A flexible statistical power analysis program for the social, behavioral, and biomedical sciences. *Behavior Research Methods*, **39**, 175–91

Flores, L.P. (2002). Occipital lobe morphological anatomy: Anatomical and surgical aspects. *Arquivos de Neuro-Psiquiatria*, **60**, 566–71

Friedrich, E.V.C., Sivanathan, A., Lim, T., et al. (2015). An Effective Neurofeedback Intervention to Improve Social Interactions in Children with Autism Spectrum Disorder. *Journal of Autism and Developmental Disorders*, **45**, 4084–4100

Friedrich, E.V.C., Zillekens, I.C., Biel, A.L., et al. (2022). Seeing a Bayesian ghost: Sensorimotor activation leads to an illusory social perception. *iScience*, **25**, 104068

Hamilton, A., Marsh, L. (2013). Two systems for action comprehension in autism: Mirroring and mentalizing. In: Baron-Cohen, Tager-Flusberg, Lombardo (eds). *Understanding Other Minds: Perspectives from developmental social neuroscience*. p. 380–96.

Herrmann, C.S., Rach, S., Neuling, T., et al. (2013). Transcranial alternating current stimulation: a review of the underlying mechanisms and modulation of cognitive processes. *Frontiers in Human Neuroscience*, **7**, 1–13

Isik, L., Koldewyn, K., Beeler, D., et al. (2017). Perceiving social interactions in the posterior superior temporal sulcus. *Proceedings of the National Academy of Sciences of the United States of America*, **114**, E9145–52

JASP Team (2019). JASP (Version 0.9.2) [Computer software]. Retrieved from https://jasp-stats.org/

Jou, R.J., Minshew, N.J., Keshavan, M.S., et al. (2010). Enlarged right superior temporal gyrus in children and adolescents with autism. *Brain Research*, **1360**, 205–12

Kanwisher, N., McDermott, J., Chun, M.M. (1997). The Fusiform Face Area: A Module in Human Extrastriate Cortex Specialized For Face Perception. *The Journal of Neuroscience*, **17**, 4302–11

Kilner, J.M., Vargas, C., Duval, S., et al. (2004). Motor activation prior to observation of a

predicted movement. *Nature Neuroscience*, **7**, 1299–1301

Kim, J.-H., Lee, J.-M., Jo, H.J., et al. (2010). Defining functional SMA and pre-SMA subregions in human MFC using resting state fMRI: functional connectivity-based parcellation method. *NeuroImage*, **49**, 2375

Kleiner, M., Brainard, D., Pelli, D. (2007). What's new in Psychtoolbox-3? In: *Perception 36 ECVP Abstract Supplement*.

Kravitz, D.J., Saleem, K.S., Baker, C.I., et al. (2014). The ventral visual pathway: An expanded neural framework for the Processing of Object Quality. *Trends in Cognitive Sciences*, **17**, 26–49

Krol, M.A., Schutter, D.J.L.G., Jellema, T. (2020). Sensorimotor cortex activation during anticipation of upcoming predictable but not unpredictable actions. *Social Neuroscience*, **15**, 214–26

von der Lühe, T., Manera, V., Barisic, I., et al. (2016). Interpersonal predictive coding, not action perception, is impaired in autism. *Philosophical Transactions of the Royal Society B: Biological Sciences*, **371**

Macmillan, N.A., Creelman, C.D. (1990). Response Bias: Characteristics of Detection Theory, Threshold Theory, and 'Nonparametric' Indexes. *Psychological Bulletin*, **107**, 401–13

Manera, V., Becchio, C., Schouten, B., et al. (2011). Communicative interactions improve visual detection of biological motion. *PLoS ONE*, **6**

Manera, V., del Giudice, M., Bara, B.G., et al. (2011). The second-agent effect: Communicative gestures increase the likelihood of perceiving a second agent. *PLoS ONE*, **6**, 1–7

Manera, V., Schouten, B., Becchio, C., et al. (2010). Inferring intentions from biological motion: A stimulus set of point-light communicative interactions. *Behavior Research Methods*, **42**, 168–78

Maranesi, M., Livi, A., Fogassi, L., et al. (2014). Mirror neuron activation prior to action observation in a predictable context. *Journal of Neuroscience*, **34**, 14827–32

McFarland, D.J., Miner, L.A., Vaughan, T.M., et al. (2000). Mu and beta rhythm topographies during motor imagery and actual movements. *Brain Topography*, **12**, 177–86

Meyer, M., Braukmann, R., Stapel, J.C., et al. (2016). Monitoring others' errors: The role of the motor system in early childhood and adulthood. *British Journal of Developmental*

Psychology, **34**, 66–85

Meyer, M.L., Taylor, S.E., Lieberman, M.D. (2015). Social working memory and its distinctive link to social cognitive ability: An fMRI study. *Social Cognitive and Affective Neuroscience*, **10**, 1338–47

Monticelli, M., Zeppa, P., Mammi, M., et al. (2021). Where We Mentalize: Main Cortical Areas Involved in Mentalization. *Frontiers in Neurology*, **12**, 1–7

Mueller-Putz, G., Scherer, R., Brunner, C., et al. (2008). Better than random: A closer look on BCI results. *International Journal of Bioelectromagnetism*, **10**, 52–55

Neri, P., Luu, J.Y., Levi, D.M. (2006). Meaningful interactions can enhance visual discrimination of human agents. *Nature Neuroscience*, **9**, 1186–92

Nitsche, M.A., Paulus, W. (2011). Transcranial direct current stimulation - Update 2011. *Restorative Neurology and Neuroscience*, **29**, 463–92

Oostenveld, R., Fries, P., Maris, E., et al. (2011). FieldTrip: Open source software for advanced analysis of MEG, EEG, and invasive electrophysiological data. *Computational Intelligence and Neuroscience*, **2011**

Van Overwalle, F. (2009). Social cognition and the brain: A meta-analysis. *Human Brain Mapping*, **30**, 829–58

Van Overwalle, F., Baetens, K. (2009). Understanding others' actions and goals by mirror and mentalizing systems: A meta-analysis. *NeuroImage*, **48**, 564–84

Palmer, C., Zapparoli, L., Kilner, J.M. (2016). A New Framework to Explain Sensorimotor Beta Oscillations. *Trends in Cognitive Sciences*, **20**, 321–23

Pascual-Marqui, R.D. (2007). Discrete, 3D distributed, linear imaging methods of electric neuronal activity. Part 1: exact, zero error localization. *arXiv:0710.3341*, 1–16

Pascual-Marqui, R.D. (2002). Standardized low resolution brain electromagnetic tomography (sLORETA): technical details. *Methods & Findings in Experimental & Clinical Pharmacology*, 1–16

Pavlidou, A., Schnitzler, A., Lange, J. (2014). Interactions between visual and motor areas during the recognition of plausible actions as revealed by magnetoencephalography. *Human Brain Mapping*, **35**, 581–92

Pavlova, M.A. (2012). Biological motion processing as a hallmark of social cognition. *Cerebral Cortex*, **22**, 981–95

Pelli, D.G. (1997). The VideoToolbox software for visual psychophysics: Transforming numbers into movies. *Spatial Vision*, **10**, 437–42

Perry, A., Troje, N.F., Bentin, S. (2010). Exploring motor system contributions to the perception of social information: Evidence from EEG activity in the mu/alpha frequency range. *Social Neuroscience*, **5**, 272–84

Pineda, J.A., Brang, D., Hecht, E., et al. (2008). Positive behavioral and electrophysiological changes following neurofeedback training in children with autism. *Research in Autism Spectrum Disorders*, **2**, 557–81

Pineda, J.A., Carrasco, K., Datko, M., et al. (2014). Neurofeedback training produces normalization in behavioural and electrophysiological measures of high-functioning autism. *Philosophical Transactions of the Royal Society: Biological Sciences*, **369**, 20130183

Quadflieg, S., Gentile, F., Rossion, B. (2015). The neural basis of perceiving person interactions. *Cortex*, **70**, 5–20

Redcay, E., Schilbach, L. (2019). Using second-person neuroscience to elucidate the mechanisms of social interaction. *Nature Reviews Neuroscience*, **20**, 495–505

Rizzolatti, G., Fogassi, L., Gallese, V. (2001). Neurophysiological mechanisms underlying the understanding and imitation of action. *Nature Reviews Neuroscience*, **2**, 661–670

Sauseng, P., Griesmayr, B., Freunberger, R., et al. (2010). Control mechanisms in working memory: A possible function of EEG theta oscillations. *Neuroscience and Biobehavioral Reviews*, **34**, 1015–22

Sauseng, P., Klimesch, W., Doppelmayr, M., et al. (2004). Theta coupling in the human electroencephalogram during a working memory task. *Neuroscience Letters*, **354**, 123–26

Sauseng, P., Klimesch, W., Schabus, M., et al. (2005). Fronto-parietal EEG coherence in theta and upper alpha reflect central executive functions of working memory. *International Journal of Psychophysiology*, **57**, 97–103

Saygin, A.P., Wilson, S.M., Hagler, D.J., et al. (2004). Point-light biological motion perception activates human premotor cortex. *Journal of Neuroscience*, **24**, 6181–88

Schilbach, L. (2016). Towards a second-person neuropsychiatry. *Philosophical transactions of the Royal Society of London. Series B, Biological sciences*, **371**, 20150081

Schilbach, L., Bzdok, D., Timmermans, B., et al. (2012). Introspective Minds: Using ALE

meta-analyses to study commonalities in the neural correlates of emotional processing, social & unconstrained cognition. *PLoS ONE*, **7**

Schilbach, L., Eickhoff, S.B., Mojzisch, A., et al. (2008). What's in a smile? Neural correlates of facial embodiment during social interaction. *Social Neuroscience*, **3**, 37–50

Schilbach, L., Timmermans, B., Reddy, V., et al. (2013). Toward a second-person neuroscience. *Behavioral and Brain Sciences*, **36**, 393–414

Schilbach, L., Wohlschlaeger, A.M., Kraemer, N.C., et al. (2006). Being with virtual others: Neural correlates of social interaction. *Neuropsychologia*, **44**, 718–30

Sliwa, J., Freiwald, W.A. (2017). Neuroscience: A dedicated network for social interaction processing in the primate brain. *Science*, **356**, 745–49

Spunt, R.P., Lieberman, M.D. (2013). The Busy Social Brain: Evidence for Automaticity and Control in the Neural Systems Supporting Social Cognition and Action Understanding. *Psychological Science*, **24**, 80–86

Stanislaw, H., Todorov, N. (1999). Calculation of signal detection theory measures. *Behavior Research Methods, Instruments, and Computers*, **31**, 137–49

Trapp, K., Spengler, S., Wüstenberg, T., et al. (2014). Imagining triadic interactions simultaneously activates mirror and mentalizing systems. *NeuroImage*, **98**, 314–23

Tzourio-Mazoyer, N., Landeau, B., Papathanassiou, D., et al. (2002). Automated anatomical labeling of activations in SPM using a macroscopic anatomical parcellation of the MNI MRI single-subject brain. *NeuroImage*, **15**, 273–89

Ulloa, E.R., Pineda, J.A. (2007). Recognition of point-light biological motion: Mu rhythms and mirror neuron activity. *Behavioural Brain Research*, **183**, 188–94

Veale, J.F. (2014). Edingburgh Handedness Inventory—Short Form: A revised version based on confirmatory factor analysis. *Laterality: Asymmetries of Body, Brain and Cognition*, **19**, 164–77

Del Vecchio, M., Caruana, F., Sartori, I., et al. (2020). Action execution and action observation elicit mirror responses with the same temporal profile in human SII. *Communications Biology*, **3**, 1–8

Wager, T.D., Smith, E.E. (2003). Neuroimaging studies of working memory: A meta-analysis. *Cognitive, Affective and Behavioral Neuroscience*, **3**, 255–74

Walbrin, J., Downing, P., Koldewyn, K. (2018). Neural responses to visually observed social interactions. *Neuropsychologia*, **112**, 31–39

Wurm, M.F., Caramazza, A. (2019). Lateral occipitotemporal cortex encodes perceptual components of social actions rather than abstract representations of sociality. *NeuroImage*, **202**, 116153

Yang, D.Y.-J., Rosenblau, G., Keifer, C., et al. (2015). An integrative neural model of social perception, action observation, and theory of mind. *Neuroscience and Biobehavioral Reviews*, **51**, 263–75

Zillekens, I.C., Brandi, M.L., Lahnakoski, J.M., et al. (2019). Increased functional coupling of the left amygdala and medial prefrontal cortex during the perception of communicative point-light stimuli. *Social Cognitive and Affective Neuroscience*, **14**, 97–107